UNIVERSITY OF BIRMINGHAM

Research at Birmingham

Reduced graphene oxide (RGO)/Mn3O4 nanocomposites for dielectric loss properties and electromagnetic interference shielding effectiveness at high frequency

Wang, Yan; Guan, Hongtao; Dong, Chenjun; Xiao, Xuechun; Du, Shangfeng; Wang, Yude

Link to publication on Research at Birmingham portal

Author's Accepted Manuscript

Reduced graphene oxide (RGO)/Mn$_3$O$_4$ nanocomposites for dielectric loss properties and electromagnetic interference shielding effectiveness at high frequency

Yan Wang, Hongtao Guan, Chenjun Dong, Xuechun Xiao, Shangfeng Du, Yude Wang
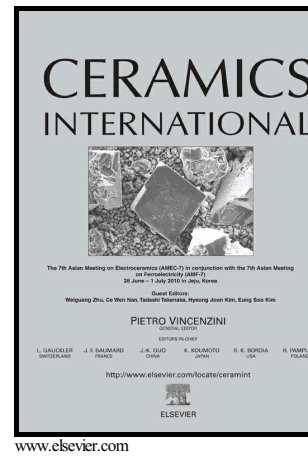
Cite this article as: Yan Wang, Hongtao Guan, Chenjun Dong, Xuechun Xiao, Shangfeng Du and Yude Wang, Reduced graphene oxide (RGO)/Mn$_3$O$_4$ nanocomposites for dielectric loss properties and electromagnetic interference shielding effectiveness at high frequency, *Ceramics International,* http://dx.doi.org/10.1016/j.ceramint.2015.09.022

This is a PDF file of an unedited manuscript that has been accepted for publication. As a service to our customers we are providing this early version of the manuscript. The manuscript will undergo copyediting, typesetting, and review of the resulting galley proof before it is published in its final citable form. Please note that during the production process errors may be discovered which could affect the content, and all legal disclaimers that apply to the journal pertain.

Reduced graphene oxide (RGO)/Mn₃O₄ nanocomposites for dielectric loss properties and electromagnetic interference shielding effectiveness at high frequency

Yan Wang,[1] Hongtao Guan,[1] Chenjun Dong, [1] Xuechun Xiao,[1] Shangfeng Du,[2,*] Yude Wang[1,3,*]

[1] Department of Materials Science and Engineering, Yunnan University, 650091 Kunming, People's Republic of China.

[2] *School of Chemical Engineering, University of Birmingham, Edgbaston, Birmingham B15 2TT, UK, E-mail: S.Du@bham.ac.uk.*

[3] *Yunnan Province Key Lab of Micro-Nano Materials and Technology, Yunnan University, 650091 Kunming, People's Republic of China.*

Abstract

Reduced graphene oxide (RGO)/Mn₃O₄ nanocomposites are prepared by a one-step hydrothermal approach and the performance of electromagnetic interference (EMI) shielding was studied. Based on an enhanced electrical conductivity through micro-current network induced by unique 2D nanostructures of RGO, the electron hopping between Mn^{2+} and Mn^{3+} is discussed. Benefiting from the enhanced effect of Debye dipolar relaxation and Maxwell-Wagner-Sillars (MWS) polarization on dielectric properties, electromagnetic wave propagating and microwave attenuation

* To whom correspondence should be addressed. Fax: +86-871-65153832; Tel: +86-871-65031124; E-mail: ydwang@ynu.edu.cn (Y. D. Wang).

performance, the maximum EMI shielding effectiveness of 29 dB is achieved.

Keywords: B. Nanocomposites; C. Dielectric properties; C. Magnetic properties; EMI shielding effectiveness.

1. Introduction

With the fast expansion of wireless data communication, local area networks, satellite television, personal digital assistants and military affairs, electromagnetic interference (EMI) has become a severe pollution, which not only influences the operation of electronic devices, but also harms the living environment for human beings. Hence, great efforts have been made to achieve high performance electromagnetic (EM) wave attenuation materials [1-9]. However, it is still a big challenge to find a material with a highly efficient electromagnetic interference (EMI) shielding performance at a light weight. Reduced graphene oxide (RGO), a two-dimensional (2D) single layer nanostructure of sp^2-compositesized carbon atoms is now well known for its extremely high specific surface areas and carrier mobilities coupling with abundant defects and hydroxyl, epoxy, and carboxyl groups in the layer. It has shown a high potential to include RGO in composites to obtain a high loss tangent and EMI shielding effectiveness [10-13]. Cao et al [14] has reported the excellent permittivity and EMI shielding performance of graphitized RGO/SiO_2 composites. Recently, the graphene-transition metal oxide nanocomposites have been explored because of their superior EM loss behaviors. For example, Xu et al [15] has investigated the dielectric loss of bowl-like Fe_3O_4 hollow sphere/RGO composites. The material with 30 wt% RGO showed a dielectric loss tangent varied from 0.18 to

2

0.64 in the frequency range of 2-18 GHz. A novel RGO/α-Fe$_2$O$_3$ composite hydrogel was fabricated by Zhang et al [16] with the maximum absorption of -33.5 dB at 7.12 GHz with a layer thickness of 5.0 mm. Cao et al [17] has also synthesized RGO-MnFe$_2$O$_4$ nanocomposites with the maximum dielectric loss tangent close to 0.6. However, although numerous graphene nanocomposites have been studied, the hybrid with the most common dielectric and microwave attenuation material Mn$_3$O$_4$ has rarely been reported.

Herein, in this work, considering the unique advantages of low cost, environmental compatibility and intrinsically high thermal stability of Mn$_3$O$_4$, we propose a facile one-step hydrothermal approach to synthesize RGO/Mn$_3$O$_4$ nanocomposites and investigate their EMI shielding effectiveness.

2. Experimental

To synthesize RGO/Mn$_3$O$_4$ nanocomposites, GO prepared by a modified Hummers method [18] was pretreated by ultrasonic vibration to form a clear homogeneous yellow brown dispersion. A typical procedure for preparing the nanocomposites was as follows: 10 ml of GO solution with a concentration of 1.5 mg/ml was mixed with 10 ml of hydrazine hydrate in a beaker. Aqueous solution of potassium permanganate was added dropwise to it under a vigorous stirring and the mixture was then stirred at room temperature for 60 min. The resulting solution was then transferred into a Teflon lined stainless steel autoclave (50 ml) and the hydrothermal process was carried out at 180 ^{o}C for 18 h. After cooling to room temperature, the dark products were rinsed with deionized water via centrifuging at a

rotation rate of 8000 r/min for several times. Finally, the as-precipitated powder was dried in a vacuum oven at 80 $^{\circ}$C. The preparation of Mn_3O_4 nanoparticles was similar to above except the addition of GO.

Powder X-ray diffraction (XRD) data were carried out by Japan Rigaku TTR-III diffractometer with Cu Kα radiation (λ= 1.5418 Å), operated at 40 kV, 100 mA. The sample was scanned from 10° to 90° (2θ) in steps of 0.01°. Scanning electron microscopy (SEM) images of the morphology of porous materials were obtained from FEI QUANTA200 with microscope operating at 30 kV. The samples for SEM were prepared by dispersing the final powders in the conductive glue; this dispersing was then sprayed with gold. Detailed studies of the microstructure were also carried out by transmission electron microscopy (TEM) (JEOL JEM-2100) at an acceleration voltage of 200 kV. Raman spectra were collected using a Renishaw InVia Raman microscope, equipped with a CCD (charge coupled device) with the detector cooled to about 153K using liquid N_2.

The electromagnetic properties of the products were characterized by the parameters of complex permittivity and permeability. The products were mixed with paraffin wax in a mass ratio of 3: 1 and then pressed into toroidal-shaped samples (Φ_{out}=7.00 mm, Φ_{in}=3.04 mm). The complex permittivity ($\varepsilon_r=\varepsilon'-j\varepsilon''$) and permeability ($\mu_r=\mu'-j\mu''$) of the mixture in the 2–18 GHz frequency range were recorded on an Agilent N5230A vector network analyzer (VNA). ε_r and μ_r represent the relative complex permittivity and permeability, respectively.

3. Results and discussion

4

Figure 1(a) shows XRD patterns of Mn_3O_4 nanoparticles and RGO/Mn_3O_4 nanocomposites. It can be seen that all the diffraction peaks of Mn_3O_4 nanoparticles were well indexed to the tetragonal phase with the space group *I4$_1$/amd* (JCPDS 24-0734, a = b =5.762 Å, c = 9.47 Å). The narrow sharp peaks confirmed that the Mn_3O_4 particle was highly crystallized. The XRD pattern of RGO/Mn_3O_4 nanocomposites was similar to the Mn_3O_4 nanoparticles except a broad peak at ca. 24°, which corresponded to RGO with the interplaner spacing of 0.34 nm [19]. The Raman spectroscopy is also an important tool to explore the structural properties of synthesized materials. The Raman spectra of GO and RGO/Mn_3O_4 nanocomposites are shown in Figure 1(b). Besides a characteristic Mn_3O_4 peak at 630 cm^{-1}, two other peaks located at the 1603 and 1361 cm^{-1} represented the G and D bands of carbon. The G band was the radial C-C stretching mode of sp^2 bonded carbon, while the D band was the first-order zone boundary phonon mode associated with the defects in the graphene or graphene edge [20]. The intensity ratio (I_D/I_G) of the D and G bands was used to qualitatively characterize the defect density of RGO before and after reduction [21]. As shown in Figure 1(b), a further increase in defect density was observed following the hydrothermal reduction procedure, with RGO/Mn_3O_4 showing more pronounced defects giving an I_D/I_G of ~1.20. This was ascribed to the significantly increase of defects on the GO nanosheets following the hydrazine reduction process [22]. Figure 1(c) and (d) show TEM and HR-TEM images of RGO/Mn_3O_4 nanocomposites, respectively. Figure 1(c) indicated a tendency of agglomeration of Mn_3O_4 nanoparticles and formation of Mn_3O_4 bulks dispersed on the

RGO nanosheets, which resulted from the existence of abundant interface between Mn_3O_4 nanoparticles. Furthermore, the RGO sheets exhibited a crumpled and rippled structure induced by the deformation during the exfoliation and restacking process. The HR-TEM image of RGO/Mn_3O_4 (Figure 1(d)) revealed the highly crystalline nature of nanoparticles and a lattice fringe with a spacing of 0.250 nm corresponding to the spacing distance of (311) planes of Mn_3O_4. The interplaner spacing of 0.341 nm was in accord with the Miller indices of (002) planes of RGO.

Figure 2(a) and (b) show the frequency dependence of the complex permeability and the complex permittivity of the Mn_3O_4 nanoparticles and RGO/Mn_3O_4 nanocomposites. The real permittivity (ε') and real permeability (μ') implied the storage ability of electric and magnetic energy of the samples, while the imaginary permittivity (ε'') and imaginary permeability (μ'') were associated with the dissipation of electric and magnetic energy [23]. As shown in Figure 2(a), because of the absence of magnetic capability in the nanoparticles, the values of μ' and μ'' of the Mn_3O_4 nanoparticles showed little fluctuation around 1 and 0, respectively. It is noteworthy that there was a negative value of μ'' for RGO/Mn_3O_4 nanocomposites, which signifies the magnetic energy radiate out without any absorption [24]. The appearance of negative value are similar to the pristine RGO reported by Wang et al [25] and it could be attributed to the inter-particle electromagnetic interaction [26]. Even though this is an impossible physical phenomenon in filler-type composite without a period superstructure, it could be achieved in practical and this unusual phenomenon has also been reported in some other works [27,28]. The existence of this rare phenomenon

suggested that the nanocomposite sample was a dielectric loss material. From Figure 2(b), it can be found that the real permittivity (ε') of the two samples decreased with increasing frequency, which could be expressed by the famous Debye equation, i.e., $\varepsilon' = \varepsilon_\infty + (\varepsilon_s - \varepsilon_\infty) / (1 + \omega^2 \tau^2)$. According to this equation, in the frequency range investigated, the decrease in ε' was attributed to the increase in angular frequency (ω). Much higher ε' for the nanocomposites than the pure Mn_3O_4 nanoparticles in the whole frequency of 2-18 GHz could be found. Meanwhile the nanocomposites showed an imaginary permittivity (ε'') of 13.9-47.9, which was also much higher than 0.007-0.08 of the pure Mn_3O_4 nanoparticles. Compared with the nearly constant ε' and ε'' within the whole frequency range for the Mn_3O_4 nanoparticles, the RGO/Mn_3O_4 nanocomposites showed a big fluctuation with both of them. The higher values of ε' and ε'' of RGO/Mn_3O_4 nanocomposites could be ascribed to the higher conductivity of RGO and Maxwell-Wagner-Sillars (MWS) polarization. According to the free electron theory, $\varepsilon'' = 1/2\,\varepsilon_0 \pi \rho f$, where ε_0 is the permittivity in vacuum, ρ is the resistivity, f is the radiation frequency [29-32], the high conductivity of RGO enabled a reduction in the resistivity of the nanocomposites, hence the imaginary dielectric constant becomes larger than that of pure Mn_3O_4. In addition, the MWS polarization, also known as the interfacial polarization, occurs when there is an accumulation of charge carriers at an interfacial between two materials. In RGO/Mn_3O_4 nanocomposites, because of the existing of touching interface between RGO and Mn_3O_4 nanoparticles and the defects/vacancies resulting from the restacking of RGO (Figure 1(c) and (d)), the free charges in graphene accumulated at the

7

interface and gave rise to a strong MWS polarization, and thus led to the enhancement of the dielectric constant.

To further understand the incident electromagnetic wave attenuation in a microwave absorbent, the dielectric loss tangent ($\tan\delta_E=\varepsilon''/\varepsilon'$) and magnetic loss tangent ($\tan\delta_M=\mu''/\mu'$) were calculated based on the measured complex permittivity and permeability. Figure 3(a) and (b) show the dielectric loss tangent and magnetic loss tangent of the Mn_3O_4 nanoparticles and RGO/Mn_3O_4 nanocomposites. For the nanocomposites, $\tan\delta_E$ was in the range of 1.10 -0.67 between 2 and 18 GHz, which is much higher than that of pure Mn_3O_4 with the largest dielectric loss of only 0.026 at 18 GHz. The excellent dielectric loss tangent properties of the nanocomposites could be concluded from the Debye dipolar polarization relaxation, interfacial polarization relaxation and the unique conductivity of RGO, etc [33,34]. First, there were dipoles with Mn_3O_4 particles, especially when their sizes were in the nanoscale. Based on the surface effect of the nanomaterial, with the decreasing in size, the number of surface atoms with unsaturated bonds increased greatly, causing an increase of the dipoles. Consequently, the dipole polarizations and electrons could not match up with the changes of EM field in the high frequency which led to the Debye relaxation contributing to the dielectric loss. Second, the vacancies at interfaces between Mn_3O_4 nanoparticles and RGO nanosheets [2,7], together with the defects on the graphene basal plane caused by the adverse excessive restacking of graphene nanosheets could act as polarized centers for the dipole polarization relaxation, enhancing the dielectric loss and electromagnetic energy dissipation [35]. Furthermore, as a result of the

8

excellent conductivity of the 2D RGO nanosheet, some conductive micro-networks and micro-capacitors could be formed in the nanocomposities leading to a reduction of resistivity and thus generated a polarization in the internal of medium. According to the free electron theory mentioned above, the ε'' became higher with the reducing of resistivity and induced an increase in dielectric loss. With the appearance of internal polarization of medium, the eddy current would occur when the polarization vector ($\vec{p}$) lagged behind the changes of electronic field and it converted the EM energy into thermal energy. In addition, such a high dielectric loss tangent could also be linked to the electron hoping between Mn^{2+} and Mn^{3+} ions through the conductivity paths constructed by the RGO as the EM wave field applied. A further demonstration of the possible mechanisms of dielectric loss of the nanocomposites is presented in Figure 4. The very low magnetic loss tangents of both samples (Figure 3(b)) indicated that the EM loss of these materials was dielectric type and the reasons for the negative value of magnetic loss tangent, is also referred.

The enhanced intrinsic electrical conductivity and dielectric constant induced by the micro-current network and MSW polarization in the nanocomposites could improve the EMI shielding effectiveness (EMI SE), which is a combined result of the reflection relative to the surface of the absorber (SE_R), the absorption of the EM energy (SE_A) and the multiple internal scattering of EM radiation (SE_M) [36]. According to the Schelkunoff formula [37] based on the Transmission line model [38,39], the EMI shielding effectiveness (SE_{total}) for a shielding material, is described by Equation (1) [37].

9

$$SE_{total} = SE_R + SE_A + SE_M \qquad (1)$$

Where SE_R, SE_A and SE_M are calculated by Equation (2), (3) and (4) as below:

$$SE_R = 168.2 + 10\lg\left(\frac{\sigma_r}{f\mu_r}\right) \qquad (2)$$

$$SE_A = 131.43t\sqrt{f\mu_r\sigma_r} \qquad (3)$$

$$SE_M = 10\lg\left[1 - 2\times10^{-0.1SE_A}\cos(0.23SE_A) + 10^{-0.2SE_A}\right] \qquad (4)$$

Where f is the microwave frequency, μ_r is the relative permeability, t is the thickness of the shielding material, σ_r is the relative conductivity of the shielding material relative to the copper. The correction term SE_M can be ignored in all practical applications when $SE_{total} > 10$ dB. On the basis of Maxwell equation, the relationship between σ_r and imaginary permittivity can be deduced as Equation (5) and (6).

$$\sigma_0 = 2\pi f\varepsilon''\varepsilon_0 \qquad (5)$$

$$\sigma_r = \sigma_0/\sigma_{cu} \qquad (6)$$

Where ε'' is the imaginary permittivity with the dimension of 1, ε_0 is the permittivity of free space with the dimension of F/m. The reflection loss (SE_R) is the result of the matching effectiveness between conductivity and magnetic permeability of the material. It indicates a larger reflection loss when there is a poor matching. On the other hand, absorption loss (SE_A) is caused by the heat loss under the action between electric dipole or magnetic dipole, which makes it clear that material with higher absorption loss performance should not only have the higher electrical conductivity but also higher magnetic permeability.

Based on Equation (1)-(6), the EMI SE of the nanocomposites and Mn_3O_4 nanoparticles versus the frequency is presented in Figure 5. It can be seen that the

10

EMI SE of the nanocomposites was much improved compared with the Mn_3O_4 nanoparticles. This improvement indicated that the enhanced conductivity resulted in poor impedance matching properties thus leading to a high reflection of incident microwave. The EMI SE of nanocomposites also increased with the frequency. Especially, when the electromagnetic wave frequency was in X (8-12 GHz) and Ku (12-18 GHz) band, the EMI SE of composites reached above 20 dB which is the target value required for commercial application.

4. Conclusion

In conclusion, the RGO/Mn_3O_4 nanocomposites with enhanced dielectric loss property have been synthesized by a one-step hydrothermal method. Attributing to Debye dipolar relaxation, electron polarization relaxation, interfacial polarization relaxation and the unique conductivity of RGO, etc, a much improved dielectric loss performance and EMI SE were achieved as compared with the pure Mn_3O_4 nanoparticles. It is believed that such nanocomposites will find applications in microwave attenuation field and can also be extended to other areas, such as lithium ion batteries and supercapacitors.

Acknowledgements

References

1. R. C. Che, L. M. Peng, X. F. Duan, Q. Chen, X. L. Liang, Microwave absorption enhancement and complex permittivity and permeability of Fe encapsulated within carbon nanotubes, *Adv. Mater.* 16 (2004) 401–405.

2. M. Zong, Y. Huang, Y. Zhao, X. Sun, C. H. Qu, D. D. Luo, J. B. Zheng, Facile preparation, high microwave absorption and microwave absorbing mechanism of RGO-Fe$_3$O$_4$ composites *RSC Adv.* 3 (2013) 23638–23648.

3. C. C. Lee, D. H. Chen, Ag nanoshell-induced dual frequency electromagnetic wave absorption of Ni nanoparticles, *Appl. Phys. Lett.* 90 (2007) 193102.

4. J. Liu, R. Che, H. Chen, F. Zhang, F. Xia, Q. Wu, M. Wang, Microwave absorption enhancement of multifunctional composite microspheres with spinel Fe$_3$O$_4$ cores and anatase TiO$_2$ shells, *Small* 8 (2012) 1214–1221.

5. Z. L. Hou, H. F. Zhou, L. B. Kong, H. B. Jin, X. Qi, M. S. Cao, Enhanced ferromagnetism and microwave absorption properties of BiFeO$_3$ nanocrystals with Ho substitution, *Mater. Lett.* 84 (2012) 110–113.

6. P. F. Guan, X. F. Zhang, J. J. Guo, Assembled Fe$_3$O$_4$ nanoparticles on graphene for enhanced electromagnetic wave losses, *Appl. Phys. Lett.* 101 (2012) 153108.

7. D. Z. Chen, G. S. Wang, S. He, J. Liu, L. Guo, M. S. Cao, Controllable fabrication of mono-dispersed RGO–hematite nanocomposites and their enhanced wave absorption properties, *J. Mater. Chem. A* 1 (2013) 5996–6003.

8. Z. P. Wu, M. M. Li, Y. Y. Hu, Y. S. Li, Z. X. Wang, Y. H. Yin, Y. S. Chen, X. Zhou, Electromagnetic interference shielding of carbon nanotube macrofilms, *Scripta Materialia* 64 (2011) 809–812.

9. M. S. Cao, J. Yang, W. L. Song, D. Q. Zhang, B. Wen, H. B. Jin, Z. L. Hou, J. Yuan, Ferroferric oxide/multiwalled carbon nanotube vs polyaniline/ferroferric oxide/multiwalled carbon nanotube mutiheterostructures for highly effective microwave absorption, *ACS Appl. Mater. Interfaces*, 4 (2012) 6948-6955.

10. A. K. Geim, Graphene: status and prospects, *Science* 324 (2009) 1530–1534.

11. M. J. Allen, V. C. Tung, R. B. Kaner, Honeycomb carbon: a review of graphene, *Chem. Rev.* 110 (2009) 132–145.

12. W. Gao, L. B. Alemany, L. J. Ci, P. M. Ajayan, New insights into the structure and reduction of graphite oxide, *Nature Chem.* 1 (2009) 403–408.

13. M. S. Cao, X. X. Wang, W. Q. Cao, J. Yuan, Ultrathin graphene: electrical properties and highly efficient electromagnetic interference shielding, *J. Mater. Chem. C* 3 (2015) 6589-6599.

14. B. Wen, M. S. Cao, M. M. Lu, W. Q. Cao, H. L. Shi, J. Liu, X. X. Wang, H. B. Jin, X. Y. Fang, W. Z. Wang, J. Yuan, Reduced graphene oxides: light‐weight and high‐efficiency electromagnetic interference shielding at elevated temperatures, *Adv. Mater.* 26 (2014) 3484–3489.

15. H. L. Xu, H. Bi, R. B. Yang, Enhanced microwave absorption property of bowl-like Fe_3O_4 hollow spheres/reduced graphene oxide composites, *J. Appl. Phys.* 111 (2012) 07A522.

16. H. Zhang, A. J. Xie, C. P. Wang, H. S. Wang, Y. H. Shen, X. Y. Tian, Novel rGO/α-Fe_2O_3 composite hydrogel: synthesis, characterization and high performance of electromagnetic wave absorption, *J. Mater. Chem. A* 1 (2013)

8547–8552.

17. X. J. Zhang, G. S. Wang, W. Q. Cao, Y. Z. Wei, J. F. Liang, L. Guo, M. S. Cao, Enhanced microwave absorption property of reduced graphene oxide (RGO)-MnFe$_2$O$_4$ nanocomposites and polyvinylidene fluoride, *ACS Appl. Mater. Interface*s 6 (2014) 7471–7478.

18. W. S. Hummers, R. E. Offeman, Preparation of graphitic oxide, *J. Am. Chem. Soc.* 80 (1958) 1339–1339.

19. J. W. Lee, A. S. Hall, J. D. Kim, T. E. Mallouk, A facile and template-free hydrothermal synthesis of Mn$_3$O$_4$ nanorods on graphene sheets for supercapacitor electrodes with long cycle stability, *Chem. Mater.* 24 (2012) 1158–1164.

20. H. L. Guo, X. F. Wang, Q. Y. Qian, F. B. Wang, X. H. Xia, A green approach to the synthesis of graphene nanosheets, *ACS Nano* 3 (2009) 2653–2659.

21. Y. Z. Xue, B. Wu, L. Jiang, Y. L. Guo, L. P. Huang, J. J. Chen, J. H. Tan, D. C. Geng, B. R. Luo, W. P. Hu, G. Yu, Y. Q. Liu, Low temperature growth of highly nitrogen-doped single crystal graphene arrays by chemical vapor deposition, *J. Am. Chem. Soc.* 134 (2012) 11060–11063.

22. S. Park, J. An, J. R. Potts, A. Velamakanni, S. Murali, R. S. Ruoff, Hydrazine-reduction of graphite-and graphene oxide, *Carbon* 49 (2011) 3019–3023.

23. W. C. Zhou, X. J. Hu, X. X. Bai, S. Y. Zhou, C. Y. Sun, J. Yan, P. Chen, Synthesis and electromagnetic, microwave absorbing properties of core–shell Fe$_3$O$_4$–poly (3, 4-ethylenedioxythiophene) microspheres, *ACS Appl. Mater. Interfaces* 3 (2011)

3839–3845.

24. C. Wang, X. Han, X. Zhang, S. Hu, T. Zhang, J. Wang, Y. Du, X. Wang, P. Xu, Controlled synthesis and morphology-dependent electromagnetic properties of hierarchical cobalt assemblies, *J. Phys. Chem. C* 114 (2010) 14826-14830

25. C. Wang, X. Han, P. Xu, X. Zhang, Y. Du, S. Hu, The electromagnetic property of chemically reduced graphene oxide and its application as microwave absorbing material, *Appl. Phys. Lett.* 98 (2011) 072906.

26. P. F. Guan, X. F. Zhang, J. J. Guo, Assembled Fe_3O_4 nanoparticles on graphene for enhanced electromagnetic wave loss, *Appl. Phys. Lett.* 101 (2012) 153108

27. D. Z. Chen, H. Y. Quan, Z. N. Huang, S. L. Luo, X. B. Luo, F. Deng, H. L. Jiang, G. S. Zeng, Electromagnetic and microwave absorbing properties of RGO@ hematite core–shell nanostructure/PVDF composites, *Compos. Sci. Technol.* 102 (2014) 126–131.

28. H. Zhang, A. J. Xie, C. P. Wang, H. S. Wang, Y. H. Shen, X. Y. Tian, Room temperature fabrication of an RGO–Fe_3O_4 composite hydrogel and its excellent wave absorption properties, *RSC Adv.* 4 (2014) 14441–14446.

29. X. Sun, J. P. He, G. X. Li, J. Tang, T. Wang, Y. X. Guo, H. R. Xue, Laminated magnetic graphene with enhanced electromagnetic wave absorption properties, *J. Mater. Chem. C* 1 (2013) 765–777.

30. Y. J. Chen, G. Xiao, T. S. Wang, Q. Y. Ouyang, L. H. Qi, Y. Ma, P. Gao, C. L. Zhu, M. S. Cao, H. B. Jin, Porous Fe_3O_4/carbon core/shell nanorods: synthesis and electromagnetic properties, *J. Phys. Chem. C* 115 (2011) 13603–13608.

31. S. He, G. S. Wang, C. Liu, J. Liu, B. Wen, H. Liu, L. Guo, M. S. Cao, Enhanced wave absorption of nanocomposites based on the synthesized complex symmetrical CuS nanostructure and poly (vinylidene fluoride), *J. Mater. Chem. A* 1 (2013) 4685–4692.

32. M. S. Cao, W. L. Song, Z. L. Hou, B. Wen, J. Yuan, The effects of temperature and frequency on the dielectric properties, electromagnetic interference shilelding and microwave-absorption of short carbon fiber/silica composites, *Carbon* 48 (2010) 788-796.

33. D. Z. Chen, G. S. Wang, S. He, J. Liu, L. Guo, M. S. Cao, Controllable fabrication of mono-dispersed RGO–hematite nanocomposites and their enhanced wave absorption properties, *J. Mater. Chem. A* 1 (2013) 5996–6003.

34. H. J. Wu, L. D. Wang, S. L. Guo, Y. M. Wang, Z. Y. Shen, Electromagnetic and microwave-absorbing properties of highly ordered mesoporous carbon supported by gold nanoparticles, *Mater. Chem. Phys.* 133 (2012) 965–970.

35. B. Wen, X. X. Wang, W. Q. Cao, H. L. Shi, M. M. Lu, G. Wang, H. B. Jin, W. Z. Wang, J. Yuan, M. S. Cao, Reduced graphene oxides: the thinnest and most lightweight materials with highly efficient microwave attenuation performances of the carbon world, *Nanoscale* 6 (2014) 5754-5761.

36. X. C. Luo, D. D. L. Chung, Electromagnetic interference shielding using continuous carbon-fiber carbon-matrix and polymer-matrix composites, *Composites Part B* 30 (1999) 227–231.

37. N. Li, Y. Huang, F. Du, X. B. He, X. Lin, H. J. Gao, Y. F. Ma, F. F. Li, Y. S. Chen,

P. C. Eklund, Electromagnetic interference (EMI) shielding of single-walled carbon nanotube epoxy composites, *Nano Lett.* 6 (2006) 1141–1145.

38. B. W. Li, Y. Shen, Z. X. Nan, Enhanced microwave absorption in nickel/hexagonal-ferrite/polymer composites, *Appl. Phys. Lett.* 89 (2006) 132504.

39. B. Wen, M. S. Cao, Z. L. Hou, W. L. Song, L. Zhang, M. M. Lu, H. B. Jin, X. Y. Fang, W. Z. Wang, J. Yuan, Temperature dependent microwave attenuation behavior for carbon-nanotube/silica composites *Carbon* 65 (2013) 124-135.

Figure 1 (a) XRD patterns of Mn_3O_4 nanoparticles and RGO/Mn_3O_4 nanocomposites; (b) Comparison of Raman spectra of the RGO/Mn_3O_4 nanocomposites and GO; (c) TEM and (d) HRTEM images of the RGO/Mn_3O_4 nanocomposites.

Figure 2 Frequency dependence of the relative complex permeability (a) and complex permittivity (b) of Mn_3O_4 nanoparticles and RGO/Mn_3O_4 nanocomposites.

Figure 3 The dielectric loss tangent (a) and magnetic loss tangent (b) of Mn_3O_4 nanoparticles and RGO/Mn_3O_4 nanocomposites, respectively.

Figure 4 The schematic of possible dielectric loss mechanisms of RGO/Mn_3O_4 nanocomposites.

Figure 5 EMI shielding effectiveness of Mn_3O_4 nanoparticles and RGO/Mn_3O_4 nanocomposites.
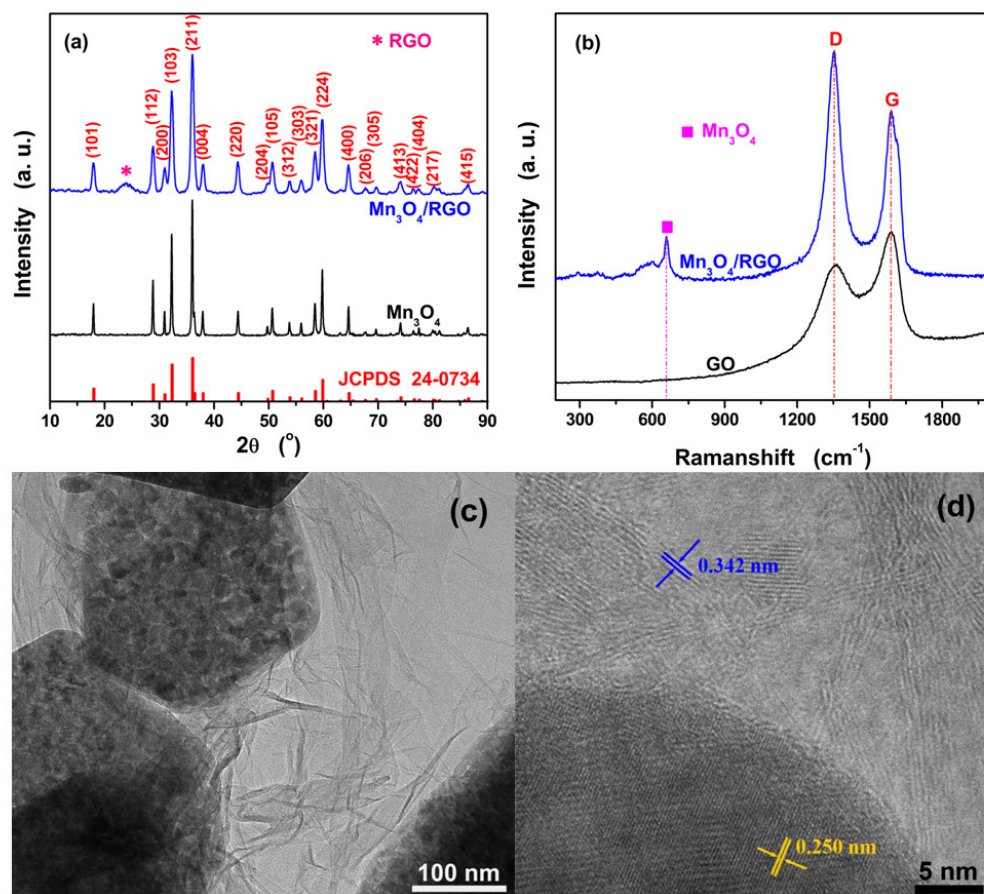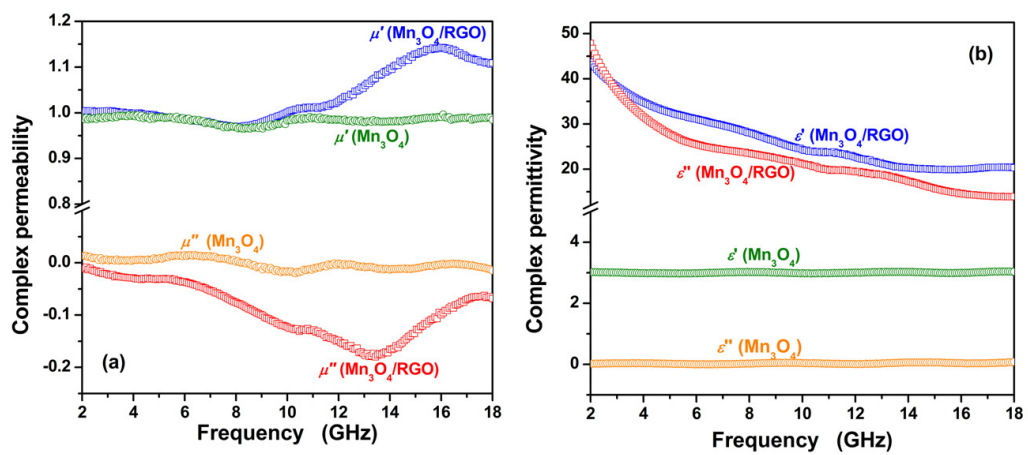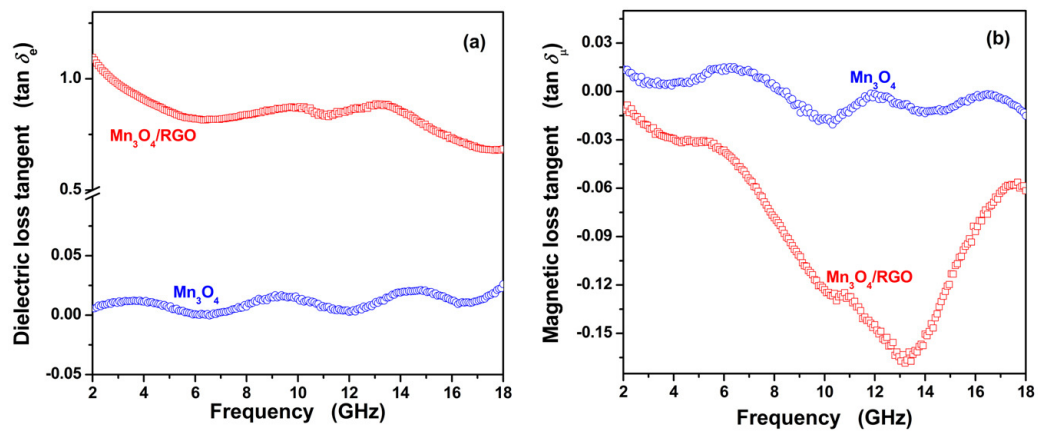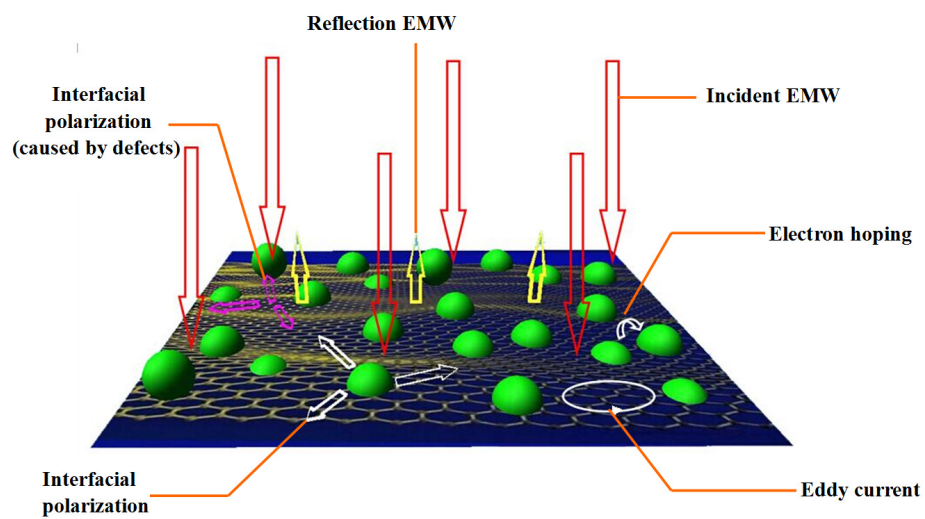
Figure 1

Figure 2

Figure 3

Figure 4

Figure 5